processes

MDPI

Article

Application of NACA 6412 Airfoil for Noise and Vibration Reduction in Evaporator Fan Blades

Aytaç Moralar * and Serhat Ekim

Mechanical Engineering Department, Tekirdag Namik Kemal University, Corlu 59830, Türkiye; serhatekim88@gmail.com

* Correspondence: amoralar@nku.edu.tr

Abstract: In today's industry, due to the importance placed on occupational health and safety, regulations are being implemented to reduce noise in factory conditions. This study aims to reduce fan noise levels while simultaneously enhancing fan efficiency. We focused specifically on the evaporator fans used in the ammonia refrigeration tunnels at Unilever's Algida ice cream production facility. Both physical and computational models of the fan blades were developed using Fluent and Phoenics computational fluid dynamics (CFD) software. Vibration analyses of the fan blades were performed using the modal analysis module. Through the analysis of pressure distributions on the existing fan blades, it was found that aerodynamic irregularities were the primary contributors to the noise. To address this, the NACA 6412 airfoil model was selected for the redesign, resulting in balanced pressure distribution across the blade surfaces and a reduction in noise levels from 96 dB to 78 dB.

Keywords: blade; CFD; fan; noise; NACA 6412

Citation: Moralar, A.; Ekim, S. Application of NACA 6412 Airfoil for Noise and Vibration Reduction in Evaporator Fan Blades. *Processes* **2024**, *12*, 2377. https://doi.org/10.3390/pr12112377

Academic Editors: Arkadiusz Gola, Izabela Nielsen and Patrik Grznár

Received: 10 October 2024
Revised: 23 October 2024
Accepted: 27 October 2024
Published: 29 October 2024

1. Introduction

A fan is a device that generates airflow by creating a pressure difference through the rotational motion derived from a mechanical energy source. The fan's moving component, the blades, performs work on the air, imparting both static and kinetic energy to it. The ratio of static to kinetic energy imparted to the air determines the characteristics of the fan. Some of the energy conversions are transformed into heat, leading to motor heating and necessitating cooling measures. Motor fans, used for cooling electric motors, have long been recognized as a primary source of noise. The need to mitigate fan noise to make motors quieter has progressively gained significance [1]. Fans can be manufactured in various types based on their usage (such as suction fans, exhaust fans, and propeller fans), the direction of airflow (radial and axial), and their capacities (blowers; bellows; and high-pressure, medium-pressure, and low-pressure fans), tailored to their respective applications [2].

Known as suction fans, aspirators operate on the principle of reducing pressure within their operating environment. These fans are employed in systems that require a mixture of indoor and outdoor air, such as those used in climate control (Figure 1a). Exhaust fans facilitate the expulsion of exhaust air equal to the amount of air being drawn in (Figure 1b). Referred to as propeller fans or blowers, centrifugal fans generate positive pressure within the air channel, imparting motion to the air and ensuring circulation of ambient air (Figure 1c). In radial fans, air is drawn through one or both sides of the radial fan blade and expelled at an angle perpendicular to the fan's shaft. Depending on blade design, radial fans can be categorized into four groups: straight, forward-curved, backward-curved, and aerodynamic blades (Figure 1d). In axial fans, air flows parallel to the fan's shaft and is expelled outward. Axial fans are further divided into two groups: those with bladed guide vanes and those with shrouds. Axial fans with guide vanes and

shrouds are often referred to as duct fans due to their tubular design. Bladed or shrouded axial fans are driven by a motor positioned either within a directly connected housing or externally in a tube casing. Duct fans are commonly constructed from galvanized sheet metal with square or rectangular profiles (Figure 1e) [2].

(**a**) (**b**) (**c**) (**d**) (**e**)

Figure 1. (**a**) Aspirator fan, (**b**) exhaust fan, (**c**) ventilator fan, (**d**) radial fan, and (**e**) axial fan [2].

Noise refers to unwanted or disruptive sounds. Sound is a mechanical wave that propagates through a vibrating medium. However, certain sound waves can be distressing to humans and other organisms. Examples of noise that can cause discomfort to humans include traffic noise, construction activities, the operation of industrial machinery, and loud music. Noise control can be achieved through environmental regulations, sound insulation, technological advancements, and societal awareness. By implementing suitable measures, noise levels can be managed, contributing to a healthier and more serene environment for individuals [3,4].

Characterizing the aerodynamic and acoustic behaviors of axial flow fans is a challenging task. Industrial fans not only often feature controlled vortex design but may also exceed catalog data on noise emissions due to the peculiarities of their configurations. A program initiated by Benedek, Vad, and Tóth aims to develop a simple method that provides design/redesign guidelines for lower noise and higher fan performance [5–7].

According to the World Health Organization (WHO), prolonged exposure to noise levels of 80 decibels (dB) presents significant health risks. Continuous exposure to noise above 70 dB is considered potentially harmful to hearing, and noise at 80 dB increases the risk of hearing damage, cardiovascular issues, and stress-related diseases. The WHO recommends that in occupational environments, noise exposure should not exceed 85 dB over an 8 h period to protect workers from hearing loss [8].

Numerous studies have been conducted in the literature to mitigate noise generated by various types of fans. Utilizing computational fluid dynamics (CFD) methodology, research has been performed on axial fans [9], condenser fans [10], radial fans [11], electric motor fans [1], automotive radiator fans [12], jet engines [13], and airflow turbulence within wind tunnels [14].

The NACA 6412 airfoil is designed to provide high lift while maintaining low drag. In this study, the goal is to reduce noise levels without compromising cooling performance. Numerous studies have been conducted using NACA-type airfoils [15,16]. Among them, the NACA 6412 airfoil was chosen for this study due to its superior pressure distribution and noise performance compared to other similar airfoil profiles.

In this study, we investigated the influence of noise sources from axial fans employed in the evaporators of ammonia refrigeration tunnels used in the Algida ice cream factory. The aim is to reduce the noise generated by low-speed axial fans commonly employed in cooling and air conditioning systems, with a specific focus on the tonal noise produced. A comprehensive literature review was conducted for the selection of the blade, and a blade profile with low drag resistance, high efficiency, and the ability to operate more effectively without reducing the output of the existing system was selected. By selecting the NACA 6412 (National Advisory Committee for Aeronautics) airfoil as the fan blade, we examined the alterations in velocity and pressure variations using a computational fluid dynamics (CFD) analysis program, thereby investigating the resultant changes in sound noise. CFD is a preferred method in engineering for understanding and simulating the behavior and

interactions of fluids. It is a powerful tool that is used under license by the company we collaborate with.

2. Materials and Methods

2.1. Cooling Tunnel

The cooling tunnel is an insulated chamber utilized in the production process of ice cream to cool and enhance the hardness of the ice cream. It operates at an ambient temperature of −42 °C, with a conveyor chain length of 550 m and a conveyor speed of 0.15 m/s. In the cooling process, facilitated by the absorption of heat from the environment by liquid ammonia, two evaporators have been incorporated. To augment the efficiency of the evaporators and the cooling capacity of the tunnel, four tunnel fans are positioned at a distance of 2.5 m from the evaporators, oriented to draw air from the evaporators (Figure 2).

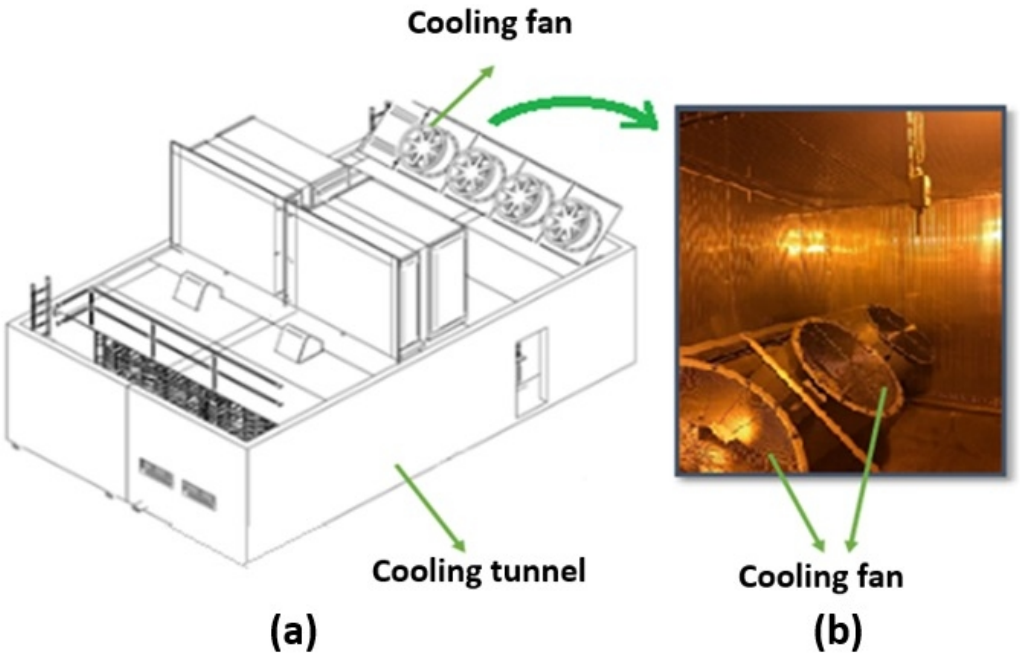

Figure 2. Cooling tunnel: schematic drawing (**a**) and actual image (**b**).

2.2. Cooling Fan

The main structure of the fan, which constitutes the primary component ensuring orderly airflow, has been fabricated from 304 stainless steel. A Siemens–branded (Siemens AG, Munich, Federal Republic of Germany) electric motor (2900 rpm, 2.2 kW, and 380 V) with a star connection and a 30 mm shaft diameter has been employed to drive the fan blades into motion. The connection between the fan blades and the motor shaft is achieved through a wedge-type coupling. Within the fan assembly, a total of 9 blades made from material P II-1000 are utilized. These blades are affixed to a two-part blade hub made of 304 stainless steel. Depending on the swallowtail engagement position in the assembly element, the blades can be adjusted to different pitch angles (15°, 30°, and 45°). For safety purposes, a protective wire mesh cover is installed at the front of the fan. An exploded view of a cooling fan is presented in Figure 3.

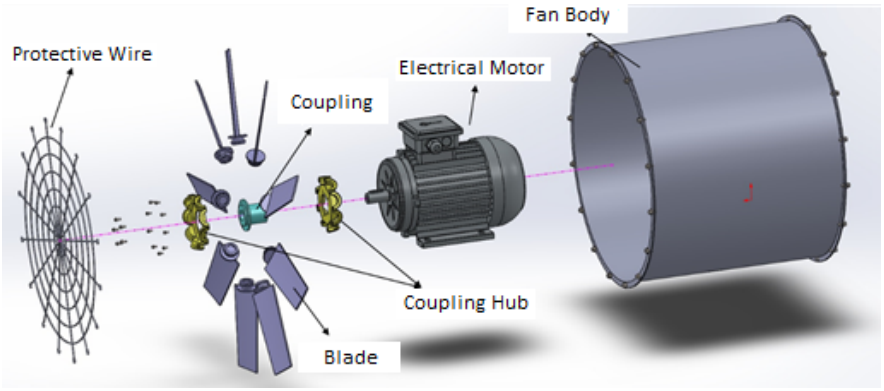

Figure 3. Exploded view of cooling fan.

2.3. Modeling and Flow Analysis

Numerous studies have been conducted in the literature using various airfoil profiles. In these studies, NACA 6412, which has the highest aerodynamic efficiency, was selected [15,16]. The new airfoil profile, NACA 6412, shown in Figure 4b, has been used to replace the previous profile illustrated in Figure 4a. The selected airfoil profile has a chord length of 100 mm, a channel thickness of 5 mm, and operates at a rotational speed of 2900 rpm.

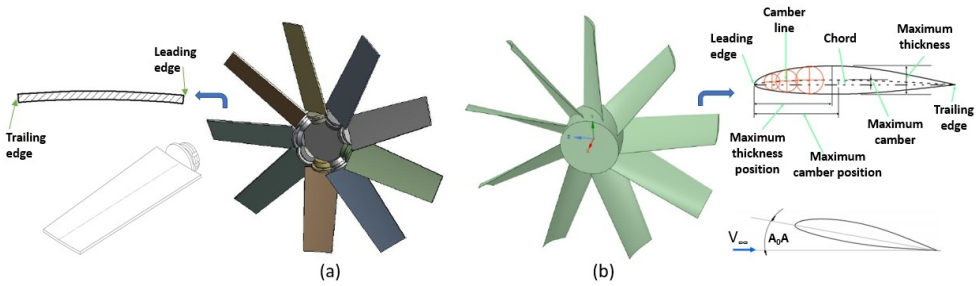

Figure 4. Old blade profile (**a**) and new blade profile (**b**).

Prior to the development of a mathematical model, necessary simplifications and assumptions were made, and the resulting flow volume is depicted in Figure 5. The 3D model, defined through geometric components using Solidworks 2013, served as the basis. The mathematical model of the system is illustrated in Figure 5a, while the numerical grid structure (mesh) is presented in Figure 5b.

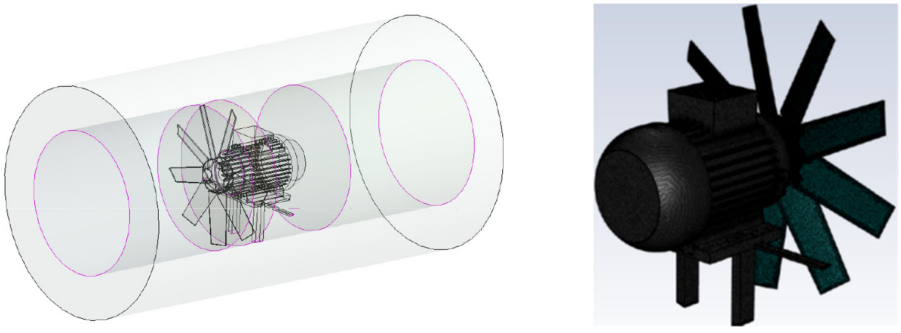

(**a**) (**b**)

Figure 5. (**a**) Flow volume and (**b**) mesh structure of flow zone.

The entire flow volume comprises approximately 9 million elements. Boundary layers were established along the surfaces of the blades and outer casing. The elements constituting the numerical grid are of the Polyhedra type.

During the numerical solution phase of the problem, the computational fluid dynamics solvers Fluent and, for verification purposes, CFD (Phoenics v3.4) software were employed. The *k*-ε turbulence model, which involves solving the transport equation for turbulent kinetic energy (*k*) and dissipation rate (ε), was selected as the turbulence model. To account for viscous effects between the turbulent region and wall regions, non-equilibrium wall functions were employed. The flow medium was defined as standard air.

The Standard *k*-ε Turbulence Model (STE) is a semi-empirical model widely utilized among two-equation turbulence models due to its cost-effectiveness and its capability to yield reasonably accurate results in various flow scenarios. When the effect of lift forces is neglected, the solution to two transport equations written for turbulent kinetic energy (*k*) and dissipation rate (ε) is provided (Equations (1) and (2)).

The derivation of the true transport equation for ε can be achieved from the Navier–Stokes equations. However, this equation is exceedingly complex and encompasses numerous unknowns. Researchers have adapted a much-simplified version, the modeled ε equation, to be employed within turbulence models. As is the case with any model, this one too involves several approximations, assumptions, and omissions [17–20].

The modeled ε transport equation is utilized in a similar form and simplified manner to the k transport equation.

$$\left\{\begin{array}{c}\text{Change amount}\\(k \text{ or } \varepsilon)\end{array}\right\}+\left\{\begin{array}{c}\text{ConvectionTransport}\\(k \text{ or}\varepsilon)\end{array}\right\}$$
$$=\left\{\begin{array}{l}\text{Difussion Transport}\\(k\text{or } \varepsilon)\end{array}\right\}+\left\{\begin{array}{c}\text{Produce amount}\\(k \text{ or } \varepsilon)\end{array}\right\}-\left\{\begin{array}{c}\text{Amount of loss}\\(k \text{ or}\varepsilon)\end{array}\right\}$$

$$\frac{\partial}{\partial t}(\rho k)+\frac{\partial}{\partial x_i}(\rho k u i_i)=\frac{\partial}{\partial x_j}\left(\Gamma_k\frac{\partial k}{\partial x_j}\right)+G_k-\rho\varepsilon \quad (1)$$

$$\tfrac{\partial}{\partial t}(\rho\varepsilon)+\tfrac{\partial}{\partial x_i}(\rho\varepsilon u_i)=\tfrac{\partial}{\partial x_j}\left(\Gamma_\varepsilon\tfrac{\partial\varepsilon}{\partial x_j}\right)+C_{1\varepsilon}\tfrac{\varepsilon}{k}G_k-C_{2\varepsilon}\rho\tfrac{\varepsilon^2}{k}-R \quad (2)$$

Diffusivity terms:

$$\Gamma_\varepsilon=\left(\mu+\frac{\mu_t}{\sigma_\varepsilon}\right)ve\,\Gamma_k=\left(\mu+\frac{\mu_t}{\sigma_k}\right) \quad (3)$$

Turbulent kinetic energy generation from the velocity gradient:

$$G_k=\mu_t\left(\frac{\partial u_i}{\partial x_j}+\frac{\partial u_j}{\partial x_i}\right)\frac{\partial u_i}{\partial x_j} \quad (4)$$

Here, μ_t is the turbulent viscosity (kg/ms), with μ, ρ, x_i, x_j, u_i, t, $C_{1\varepsilon}$, $C_{2\varepsilon}$, C_μ, G_k, R, Γ_ε, σ_k, and σ_ε.

$$\mu_t=\rho C_\mu\frac{k^2}{\varepsilon} \quad (5)$$

In this model, the R is 0, with the experimental constants being specified as follows: $C_{1\varepsilon}=1.44, C_{2\varepsilon}=1.92$, and $C_\mu=0.09$. The turbulence Prandtl numbers for k and ε are sequentially assigned $\sigma_k=1.0$ and $\sigma_\varepsilon=1.3$, as reported by [4,21,22].

To account for the viscous effects between the turbulent region and the wall zones, a non-equilibrium wall function approach was adopted. The flow entity was characterized as standard air.

Shown in Figure 6, the flow model of the provided fan was utilized to compute pressure, velocity, force, and streamlines developed on the blades and motor casing. The fan was operated at 2900 rpm under atmospheric conditions.

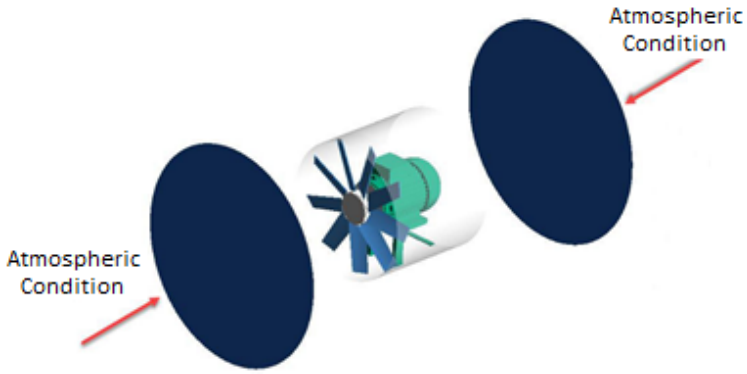

Figure 6. Computational fluid dynamics model.

Two separate regions, a rotating zone and a non-rotating zone, were created. This zoning was implemented to independently address the effects of rotating and stationary components on the flow. The connection between the rotating and non-rotating zones was established using an interface.

In this context, the Frozen Rotor method was employed to ensure accurate transfer of flow parameters between the rotating and stationary zones. The Frozen Rotor method considers the effects of relative velocities between the two zones, enabling effective modeling of their interaction. This method ensures that momentum, energy, and other fluid properties are reliably transferred across the interface, allowing for a comprehensive analysis of the effects of both regions on the flow.

Such a coupling and zoning approach allows for accurate modeling of the influence of rotating elements on the flow, providing a more precise analysis of the system's performance.

To ensure accurate modeling of the boundary layer near the fan walls, the y+ values were kept between 1 and 30. The boundary layer thickness was calculated using the CFD Online y+ calculator, and this value was applied to the model. For the mesh structure, a denser mesh was used near the blades to achieve precise results, while a coarser mesh was applied in the distant regions where finer details were less critical. This approach struck a balance between accuracy in key areas and computational efficiency.

The inlet distance was set to 3D, where D is the diameter of the fan, measured from the fan inlet to the boundary of the inlet region. This distance was chosen to ensure sufficient flow development in the inlet region. The outlet distance was set to 7D to ensure that the effects of the fan were adequately dispersed in the outlet region and to provide sufficient distance for balancing the flow effects.

The model was divided into rotating and stationary regions. The size of the area surrounding the fan was maintained large enough to allow for unobstructed movement of the flow around the fan and to ensure that the boundary conditions did not affect the accuracy of the solution.

The fan rotation was simulated using the moving mesh technique. This method allows for the dynamic movement of the mesh to account for the fan's rotation, providing a more accurate representation of the rotating flow field.

2.4. Measurement of Sound Noise

The measurement of acoustic noise was conducted using the Cesva SC 310 model measurement device. This instrument is in accordance with the DIN-EN 415-9 [23] standard, which outlines the noise measurement method for packaging machines. The measurement procedures were carried out following the guidelines specified in this standard.

3. Findings and Discussion

3.1. Pressure Values

According to the data obtained from the analysis, the pressure values on the leading edge of the blade surface are presented in Figure 7, while the pressure values on the trailing

edge of the blade surface are depicted in Figure 8. The results indicate that the maximum pressure occurs at the blade tips, where they are furthest from the center and experience the fastest interaction with the surrounding air.

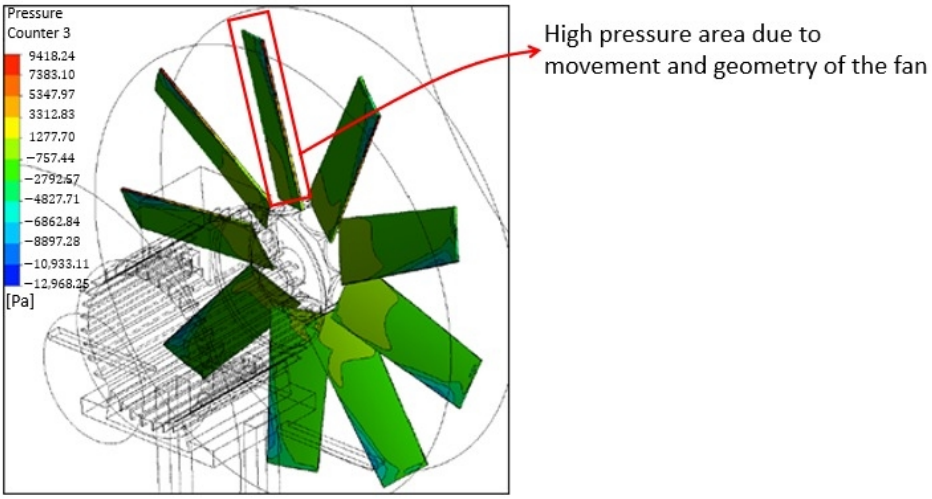

Figure 7. Front region of the blade's pressure values.

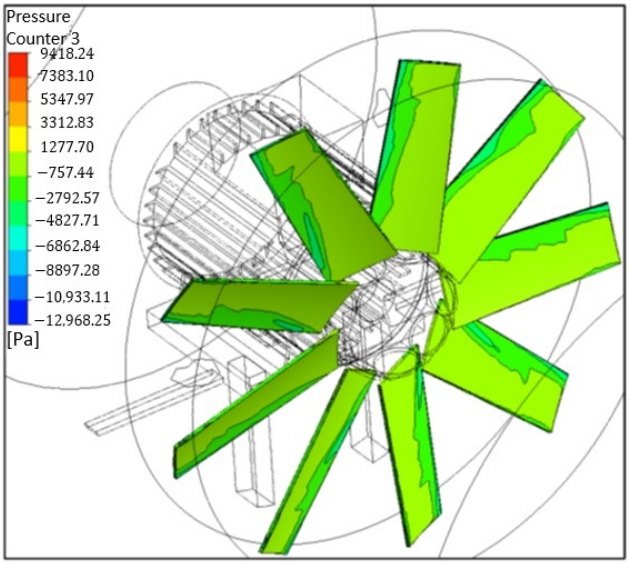

Figure 8. Rear region of the blade's pressure values.

Furthermore, it was observed that the regions of the fan blade situated on the opposite side of the flow direction experienced negative pressure relative to the atmosphere.

Figure 9a shows the point where pressure measurements were taken on the blade profile (red dot). Figure 9b presents a visualization of the pressure distributions on the blade profile (blue zones). Figure 9c provides a detailed view of the pressure and vacuum regions. Examining the pressure gradient on the rear (motor-facing) and front surfaces of the blade, it is observed that the maximum pressure is 9.4 kPa and the minimum pressure was -13 kPa. Additionally, positive pressure is located at the edge separating the flow. The analysis reveals the development of an axial force of 199 N on the fan. Furthermore, the calculated value for the torque generated at the motor shaft is 54 Nm.

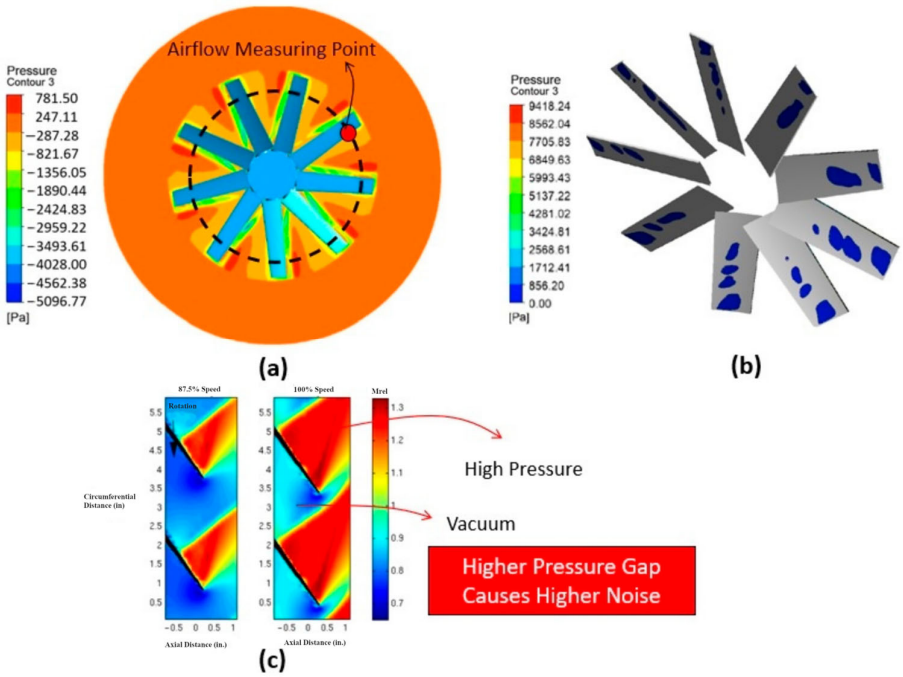

Figure 9. Pressure and vacuum regions on the blade profile: pressure measurement point (**a**), pressure visualization on the blade (**b**), and detailed view of the pressure and vacuum regions (**c**).

The effects of rotational speed and fan blade geometry on noise generation were observed. The angle and pitch of the fan blades not only influence airflow capacity but also affect the intensity of the noise produced. The cross-sectional area of the fan blades oriented perpendicular to the airflow, along with their geometric design, leads to an uneven pressure distribution between the blades, as seen in Figure 10. This variation also creates high- and low-pressure zones in the surrounding air, contributing to noise generation.

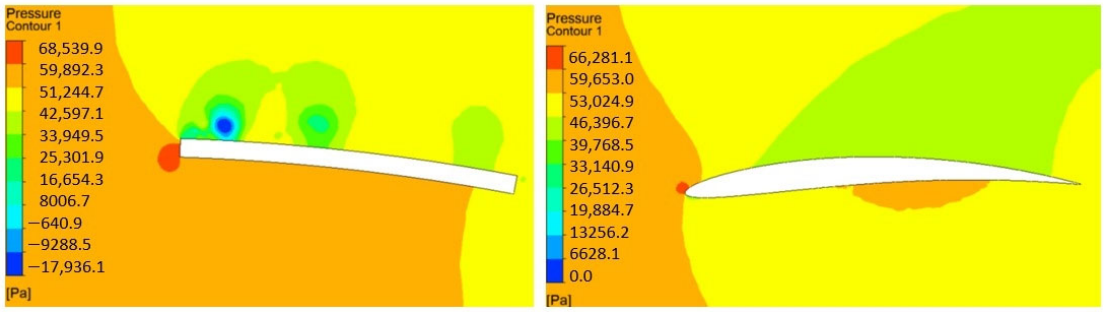

Figure 10. Pressure distribution on the fan blades: old blade profile (**a**) and new blade profile (**b**).

Due to the linearity of the fan blade angle, the minimum tangential velocity is closest to the center, while the maximum tangential velocity is at the furthest point. This causes pressure differences between the center and tangential points within the flow tunnel, thereby increasing noise levels.

According to the results of the dynamic analysis, the pressure variation graph occurring at a fixed point in the air during one complete revolution of the propeller is illustrated in Figure 10, along with the measurement point. It now illustrates the pressure differences that occur on the fan profiles during a full rotation. In the old fan model, the pressure amplitude averaged 80 Pa, while in the new fan, this value was reduced to an average of 40 Pa. Pressure amplitude is a key factor in determining the energy and intensity of sound,

particularly noise or acoustic waves. It refers to the magnitude of pressure fluctuations that occur due to the movement of air molecules.

Pressure amplitude directly influences sound intensity, noise level, and acoustic energy. Simply put, the higher the pressure amplitude, the stronger and louder the sound. Therefore, in aerodynamic applications or acoustic studies, the amplitude of pressure fluctuations plays a critical role in noise control. In Figure 11a, the pressure amplitude of the old fan is shown to be higher than that of the new fan in Figure 11b, demonstrating that the new fan design successfully reduces noise.

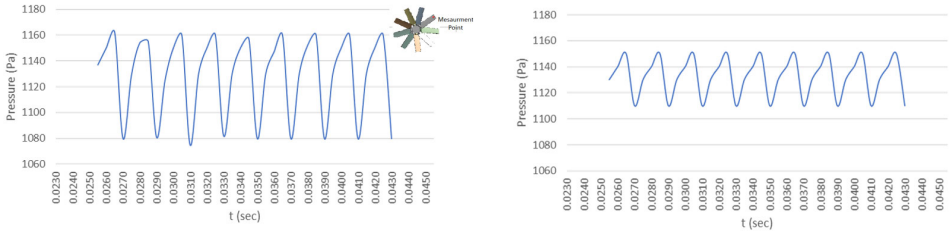

Figure 11. Graphic of pressure gradient (old fan (**a**) and new fan (**b**)).

The amplitude of the air pressure variation directly influences the intensity of the noise. Amplitude and noise intensity are directly proportional.

A frequency of 555 Hz for the noise was determined during the 0.0018 period between peak points. According to the noise measurement results, the highest noise occurred in the range of 400–600 Hz. The analysis results confirm this observation.

3.2. Velocity Distribution

Figure 12 displays the regions between the fan blades and the motor, as well as the reverse flow vectors on the motor. The axial air velocity is 62 m/s, and the fan outlet mass flow rate is determined as 19.7 kg/s.

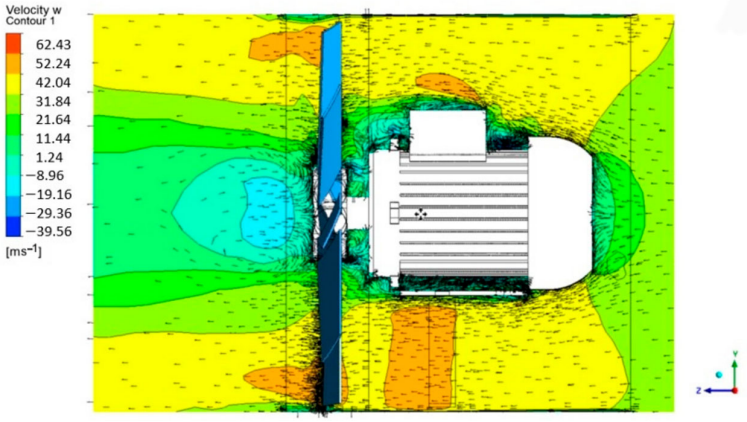

Figure 12. Velocity vectors and velocity distribution.

Figure 13 illustrates the velocity distribution in the midsection of the fan. Here, the influence of the tangential velocity of the fan blade on the airflow velocity is identified. Due to the linear nature of the fan blade angle, it is observed that the flow velocity increases as one moves away from the center. Consequently, a homogeneous flow cannot be achieved, and noise is generated due to the resulting pressure differential.

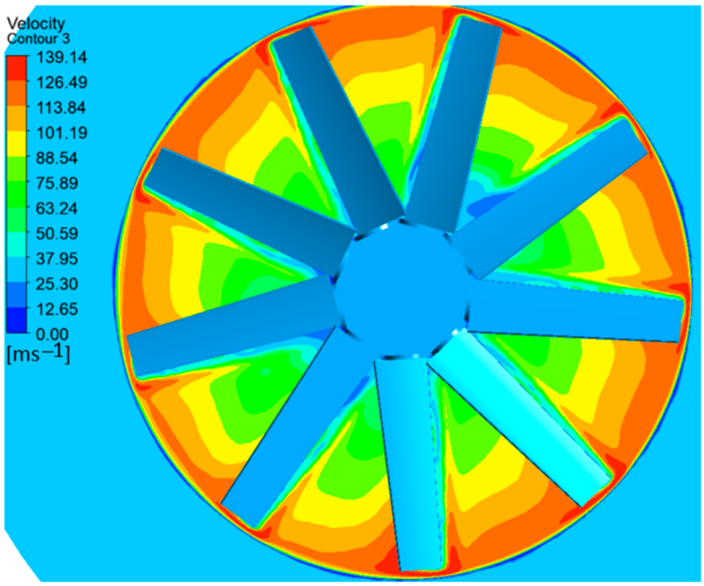

Figure 13. Velocity distribution in the midsection of the fan.

As shown in Figure 14, the air velocity variations on the current fan blade are higher compared to the new fan blade. Sudden pressure changes lead to vibrations, which increase noise levels. Additionally, as the velocity increases toward the blade tips, the pressure in these regions reaches its lowest levels. These pressure differentials across the blade are a significant factor in noise generation. It was observed that the velocity variation on the new blade profile was less pronounced compared to the old blade, and the reduction in pressure differentials led to decreased noise levels.

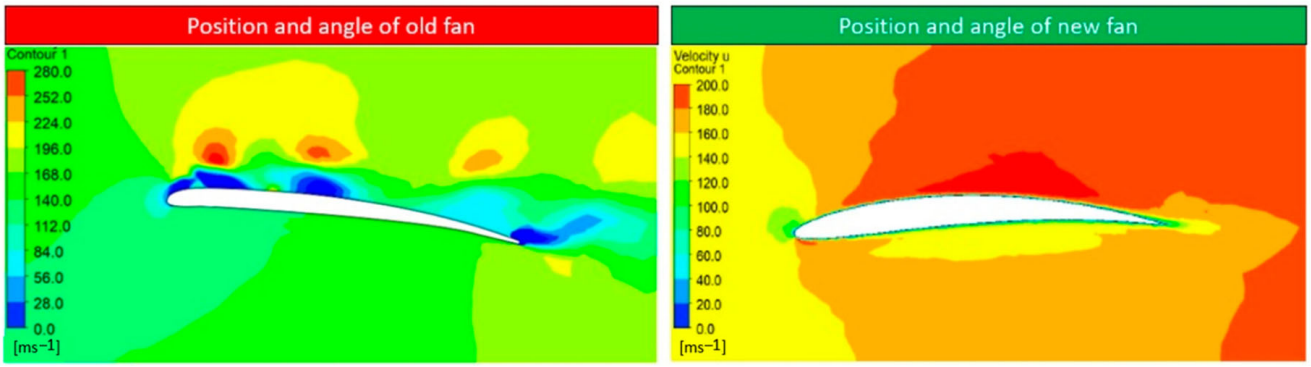

Figure 14. Air velocity distributions on old and new blade surfaces.

3.3. Noise Measurement Results

According to the noise measurement results, the highest noise levels occurred in the 400–600 Hz range. In this range, the noise intensity for the old fan blades was measured at 96 dB. In contrast, for the NACA 6412-type blades, the highest noise level was observed in the 45–50 Hz range, dropping to 78 dB. In accordance with noise regulations, the exposure limit for workers is set at 85 dB [24,25]. It is noteworthy that the noise level, which initially exceeded this critical threshold, was effectively reduced below the limit with the new design (Figure 15).

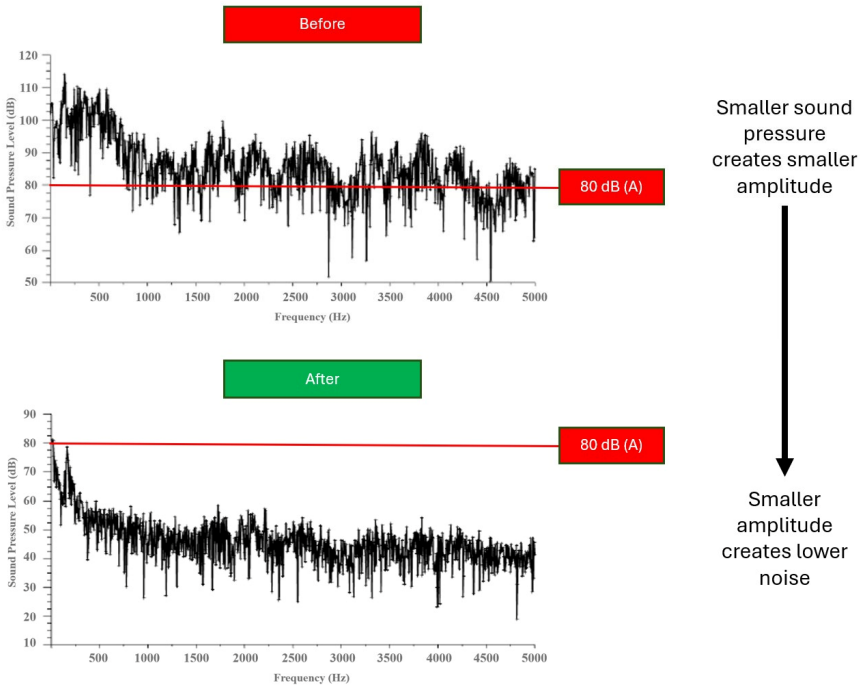

Figure 15. Noise measurement graphic of old and new fans.

The most effective outcome of the system's operational data is its cooling performance. No reduction in cooling performance was detected, indicating that the selected blade profile was designed to maintain optimal performance. To keep the focus of this study intact, detailed information regarding cooling performance has not been provided. This approach allows for a more concentrated analysis of other factors influencing the system's efficiency.

In addition, the fans within the factory machinery area that may cause noise are shown in Area 1 on a layout map. The results of the sound measurements taken before and after the study, using a Cesva SC 310 model sound measurement device (CESVA Instruments, SL., Barcelona, Spain), are presented in Figure 16. In the figure, it can be observed that the noise level has been reduced to values that do not affect human health, as determined by the World Health Organization. The intensity of the sound level is scaled using the color scale provided in Figure 16.

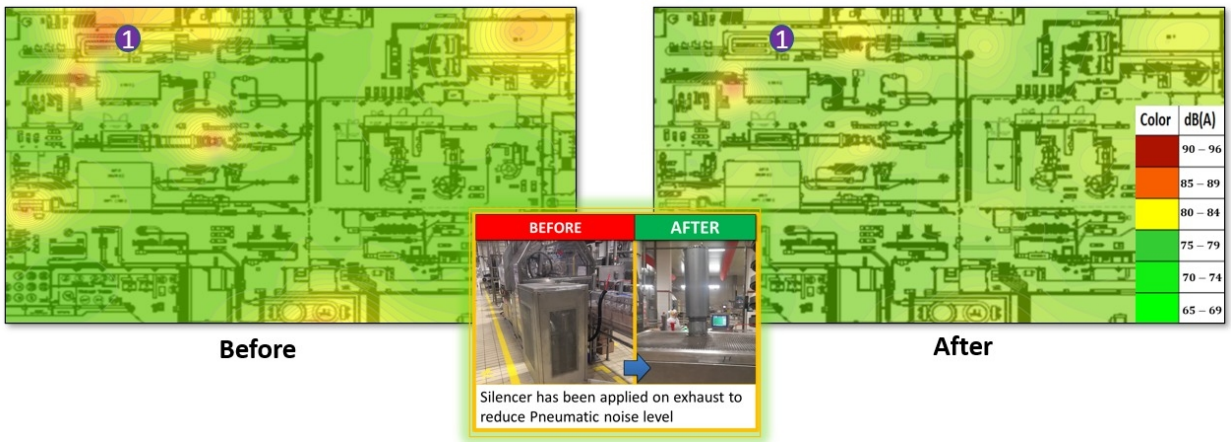

Figure 16. Noise measurement result.

4. Vibration Analysis

Vibration analyses of the fan blades were conducted using the modal analysis module to better understand the mechanical properties of the fan and to determine its vibration

responses. Table 1 presents the resonance frequencies associated with the fan. Additionally, Table 2 provides the Campbell Diagram data for six different speeds of the fan. Modal analysis is an engineering tool used to identify the fundamental vibration modes and frequencies of a system or structure. In this analysis, the relationship between the natural frequency of the fan blades and the frequency of noise produced by the fan's operational speed was examined to identify any harmonic interactions. It is predicted that sound noise levels will increase at frequency ranges where the natural vibration frequencies obtained from modal analysis align with the noise frequencies generated by the system's operational speed. The natural vibration frequencies obtained from the modal analysis were found to closely match the critical speeds of the system (2900 rpm). This observation indicates that vibration is one of the primary factors contributing significantly to the noise generated during operation.

Table 1. Natural frequencies.

Mode	Frequency (Hz)
1	24.514
2	32.338
3	47.779
4	48.568
5	49.065
6	50.329

Table 2. Campbell Diagram data.

Mode	Whirl Direction	Mode Stability	Critical Speed (rpm)	1500 (rpm)	2000 (rpm)	2900 (rpm)	3000 (rpm)	3500 (rpm)
1	BW	STABLE	NONE	24.514	21.981	18.276	17.251	16.314
2	BW	STABLE	1940.3	32.338	32.338	32.337	32.337	32.337
3	FW	STABLE	2851.9	47.779	47.704	47.522	47.456	47.39
4	FW	STABLE	2929.4	48.568	48.766	48.823	48.832	48.839
5	BW	STABLE	2960.9	49.065	49.169	49.336	49.398	49.463
6	FW	STABLE	NONE	50.329	55.87	67.147	71.133	75.213

5. Conclusions

The angle and inclination of the fan blade not only affect the airflow capacity but also influence the intensity of noise. The cross-sectional area and geometric structure of the blade in the direction perpendicular to the airflow result in a non-uniform pressure distribution on the blade. This, in turn, leads to the formation of positive and negative pressure regions in the air. Continuous pressure and velocity changes between the fan and the motor compress the fluid in that region, causing vibration and noise.

Due to the linear nature of the blade angle, the minimum tangential velocity occurs closest to the center, while the maximum tangential velocity occurs farthest from the center. This phenomenon creates a pressure difference at the center and tangential points within the airflow tunnel, contributing to increased noise.

The stress at the point where the blade separates the airflow has been minimized by altering the blade geometry. Additionally, designing the blade angle to decrease tangentially from the center reduces both turbulence and recirculation regions on the motor housing and the blade itself, thereby diminishing instantaneous fluctuations. It has been observed that the blade geometry plays a critical role in the generation of noise caused by airflow.

Furthermore, it has been determined that the distance between the motor and the blades creates turbulence and backflow regions on both the motor housing and the blades, resulting in intermittent fluctuations.

While reducing noise levels that have significant effects on human health, there was no loss in cooling performance. The airflow rate in the cooling duct was monitored before

and after the modifications, and since no loss that would diminish cooling performance was observed, no additional data have been presented in this study.

In this study, the use of the NACA 6412-type blade was deemed suitable for achieving a homogeneous pressure distribution on the blade surface. The newly selected fan model exhibited balanced pressure distributions, reducing noise levels from 96 dB to 78 dB. As a result, the noise level was brought below the WHO standard of 85 dB, ensuring appropriate working conditions. It is recommended that the chosen blade profile be adopted in industries utilizing cooling fans.

Author Contributions: Conceptualization, A.M. and S.E.; methodology, A.M.; software, S.E.; validation, A.M. and S.E.; formal analysis, A.M.; investigation, S.E.; resources, S.E.; data curation, A.M.; writing—original draft preparation, A.M.; writing—review and editing, A.M.; visualization, S.E.; supervision, A.M.; project administration, A.M. All authors have read and agreed to the published version of the manuscript.

Funding: This research received no external funding.

Data Availability Statement: The authors state that data will be available upon request. This study is derived from a MSc Thesis (ID: 582296).

Acknowledgments: We would like to thank the Unilever Çorlu Algida factory for providing the laboratory facilities.

Conflicts of Interest: The authors declare no conflicts of interest.

References

1. Rama Krishna, S.; Rama Krishna, A.; Ramji, K. Reduction of motor fan noise using CFD and CAA simulations. *Appl. Acoust.* **2011**, *72*, 982–992. [CrossRef]
2. Ekim, S. Reduction of the Noise Generated from Evaporation Fans Inside Ammonia Cooling Tower. Master's Thesis, Graduate School of Natural and Applied Sciences, Tekirdağ Namık Kemal University, Tekirdağ, Türkiye, 2019.
3. Cattanei, A.; Ghio, R.; Bongiovı, A. Reduction of the tonal noise annoyance of axial flow fans by means of optimal blade spacing. *Appl. Acoust.* **2007**, *68*, 1323–1345. [CrossRef]
4. Jiang, B.; Wang, J.; Yang, X.; Wang, W.; Ding, Y. Tonal noise reduction by unevenly spaced blades in a forward-curved-blades centrifugal fan. *Appl. Acoust.* **2019**, *146*, 172–183. [CrossRef]
5. Kalmár-Nagy, T.; Dezső Bak, B. Vibration and Noise of an Axial Flow Fan. *Period. Polytech. Mech. Eng.* **2015**, *59*, 109–113. [CrossRef]
6. Benedek, T.; Vad, J. Concerted Aerodynamic and Acoustic Diagnostics of an Axial Flow Industrial Fan, Involving the Phased Array Microphone Technique. In Proceedings of the ASME Turbo Expo 2014: Turbine Technical Conference and Exposition, Düsseldorf, Germany, 16–20 June 2014.
7. Tóth, B. *Phased Array Microphone Measurement of an Axial Flow Fan*; BME Department of Fluid Mechanics: Budapest, Hungary, 2014.
8. *World Report on Hearing*; World Health Organization: Geneva, Switzerland, 2021.
9. Wu, Y.; Pan, D.; Pen, Z.; Ouyan, H. Blade force model for calculating the axial noise of fans with unevenlyspaced blades. *Appl. Acoust.* **2019**, *146*, 429–436. [CrossRef]
10. Angelini, G.; Bonanni, T.; Corsini, A.; Delibra, G.; Tieghi, L.; Volponi, D. Optimization of an axial fan for air cooled condensers. *Energy Procedia* **2017**, *126*, 754–761. [CrossRef]
11. Moreau, S.; Sanjosé, M.; Magne, S. Optimization of tonal noise control with flow obstruction. *J. Sound Vib.* **2018**, *437*, 264–275. [CrossRef]
12. Kudo, T.; Tominaga, T.; Eguchi, T.; Suzuki, A. Development of Noise Reduction Method for Radiator Fun of Automobile. In Proceedings of the JSME Annual Meeting, Fukuoka, Japan, 4 September 2004.
13. Pochkin, Y.; Khaletskiy, Y. Aircraft fan noise reduction technology using leaned stator blades. *Procedia Eng.* **2015**, *106*, 368–376. [CrossRef]
14. Wang, C. Noise source analysis for two identical small axial-flow fans in series under operating condition. *Appl. Acoust.* **2017**, *129*, 13–26. [CrossRef]
15. Zaheer, Z.; Reby Roy, K.E.; Nair, G.S.; Ragipathi, V.; Niranjan, U.V. CFD analysis of the performance of different airfoils in ground effect. *J. Phys. Conf. Ser.* **2019**, *1355*, 012006. [CrossRef]
16. Khairani, T.C.; Marpaung, T.J.; Suriati. Computational Analysis of Fluid Behaviour Around Airfoil with Navier-Stokes Equation. In Proceedings of the 2018 International Conference on Engineering, Technologies, and Applied Sciences, Bandar Lampung, Indonesia, 18–20 October 2018.

17. Davidson, E.J. *Evaluation Methodology Basics: The Nuts and Bolts of Sound Evaluation*; SAGE Publications: Thousand Oaks, CA, USA, 2005.
18. Yang, T.; Xiaolan, C.; Cheng, H. Aerodynamic Performance Analysis of Axial-fan in Low Pressure Pipeline based on ANSYS CFX. In Proceedings of the Joint International Mechanical, Electronic and Information Technology Conference (JIMET 2015), Chongqing, China, 18–20 December 2015.
19. Kalkan, O.O. Implementation Of K-Epsilon Turbulence Models in a Two Dimensional Parallel Navier-Stokes Solver on Hybrid Grids. Master's Thesis, The Graduate School of Natural and Applied Sciences of Middle East Technical University, Ankara, Türkiye, 2014.
20. Huang, B.; Xu, J.; Wang, J.; Xu, L.; Chen, X. Numerical Investigation on the Aerodynamic and Aeroacoustic Characteristics in New Energy Vehicle Cooling Fan with Shroud. *Process* **2024**, *12*, 333. [CrossRef]
21. Zhang, Y.; Rahman, M.M.; Chen, G. Development of k-R turbulence model for wall-bounded flows. *Aerosp. Sci. Technol.* **2020**, *98*, 105681. [CrossRef]
22. Jian, C.; Yuan, H.; Li, G.; Canxing, W.; Liu, C.; Yuanrui, L. Aerodynamic noise prediction of a centrifugal fan considering the volute effect using IBEM. *Appl. Acoust.* **2018**, *132*, 182–190.
23. *DIN EN 415-9*; Safety of Packaging Machines—Part 9: Noise Measurement Methods for Packaging Machines, Packaging Lines and Associated Equipment, Grade of Accuracy 2 and 3. European Standards: Brussels, Belgium, 2009.
24. Fink, D.J. What Is a Safe Noise Level for the Public? *Am. J. Public Health* **2017**, *107*, 44–45. [CrossRef] [PubMed]
25. Şahinoğlu, A.; Rafighi, M.; Kumar, R. An investigation on cutting sound effect on power consumption and surface roughness in CBN tool-assisted hard turning. *Proc. IMechE Part E J. Process Mech. Eng.* **2022**, *236*, 1096–1108. [CrossRef]